Optical transmission in triple-film hetero-opals

W. Khunsin, S. G. Romanov' , C. M. Sotomayor Torres, J. Ye, and R. Zentel

Citation: Journal of Applied Physics **104**, 013527 (2008); doi: 10.1063/1.2951958
View online: http://dx.doi.org/10.1063/1.2951958
View Table of Contents: http://aip.scitation.org/toc/jap/104/1
Published by the American Institute of Physics

Optical transmission in triple-film hetero-opals

W. Khunsin,[1] S. G. Romanov,[1,2,a)] C. M. Sotomayor Torres,[1,3] J. Ye,[4] and R. Zentel[4]
[1]*Tyndall National Institute, University College Cork, Lee Maltings, Cork, Ireland*
[2]*Ioffe Physical Technical Institute, 194021, Polytekhnicheskaya ul., 26, St. Petersburg, Russia*
[3]*Catalan Institute for Research and Advanced Studies, ICREA, 08010 Barcelona and Catalan Institute of Nanotechnology, Edifici CM7, Campus Universitat Autonoma de Barcelona, 08193 Bellaterra, Spain*
[4]*Institute of Organic Chemistry, University of Mainz, Mainz, Germany*

(Received 29 February 2008; accepted 28 April 2008; published online 11 July 2008)

Angle-resolved transmission of *s*-polarized light in triple-film hetero-opals has been investigated in the spectral range including high-order photonic band gaps, and compared to the transmission of its constituent single-film opals. The interfaces do not destroy the predominantly ballistic light propagation over the studied frequency and angular ranges, but heterostructuring leads to a smoothed angular distribution of intensity of the transmitted light and to the reconstruction of the transmission minima dispersion. The interface transmission function has been extracted by comparing the transmission of the hetero-opal and its components in order to demonstrate the difference. This deviation from the superposition principle was provisionally assigned to light refraction and reflection at the photonic crystal interfaces and to the mismatch between mode group velocities in hetero-opal components. © *2008 American Institute of Physics*.
[DOI: 10.1063/1.2951958]

I. INTRODUCTION

A search for new possibilities of light flow manipulation is a current trend in the development of photonic crystals (PhCs). In order to exploit the full potential of PhCs, optical elements based on three-dimensional (3D) PhCs are highly desirable. Various fabrication methods have been proposed to meet this technological challenge: silicon-processing technique,[1] wafer-fusion technique,[2] autocloning,[3] holographic lithography,[4] micromanipulation,[5] and direct laser writing.[6] Among others, self-assembled colloidal crystals,[7–9] which are collectively called *artificial opals*, are the most widely studied 3D PhCs to date. Owing to their relatively straightforward and cost-effective preparation technique, opals are often considered as a benchmark for 3D PhCs prepared by other methods. In addition, opals can be used as PhCs with directional photonic band gaps (PBGs) or as templates for infiltration with high refractive index (RI) materials to obtain a theoretically predicted omnidirectional PBG.[10]

New functions can be achieved by incorporation of deterministic artificial defects in opal-based PhCs. Taking into account the limited flexibility of self-assembly, the first step can be the preparation of hetero-opals[11–15] incorporating planar defects.[16,17]

A natural way of understanding new features is to compare the PBG properties in hetero-opals to those of the single-film opals over a wide spectral range including high-order PBGs.[18,19] The obvious consequence of assembling a heterostructure from opals with different lattice constants is the accumulation of PBG features originating from each film in the measured transmission spectrum. Whether the resulting spectrum is a linear superposition of partial transmission spectra from opal films, or whether new transmission features will appear due to complex wave propagation in a hetero-opal, is a question of genuine importance for the implementation of hetero-PhCs in photonic devices. Examples of such collective effects are the transmission oscillations in opal superlattices[12] and a localized PBG transmission mode of a planar defect.[20] Apparently, the transmission variation becomes a function of the interface topology, which is characterized by the PhC truncation, the separation between the films at the heterojunction, the interface disorder and the lattice period mismatch between crystals in a hetero-opal. The finite-difference time-domain modeling of the two dimensional PhC heterojunction suggested, for example, the stronger suppression of light propagation in the frequency range of high-order gaps compared to that in the frequency range of the Bragg gap, and the partial freezing of light flow in a form of standing waves in a hetero-PhC.[21]

The aim of this paper is to examine the transmission properties of a triple-film opal PhC, which consists of a stack of opal PhCs with slightly different lattice periods, namely, a film of larger lattice constant sandwiched between two films of smaller lattice constant. The content is focused on the changes in the transmission characteristics associated with the internal heterointerfaces. We studied the transmission of the triple-film hetero-opal and the single-film opals in a wide spectral range including several band gaps and over a broad angular range of light incidence. It was observed that the light propagation in hetero-opals follows the PBG structures of each film and obeys the superposition principle in the low frequency range near the Bragg gaps, but deviates from the superposition in the range of high-order bands.

The paper is organized as follows: Sec. II describes sample preparation and details of the optical characterization technique. Section III discusses the transmission spectra. An overview of transmission changes is presented in Sec. IV. In Sec. V the dispersions of transmission minima for the single

a)Electronic mail: sergei.romanov@tyndall.ie.

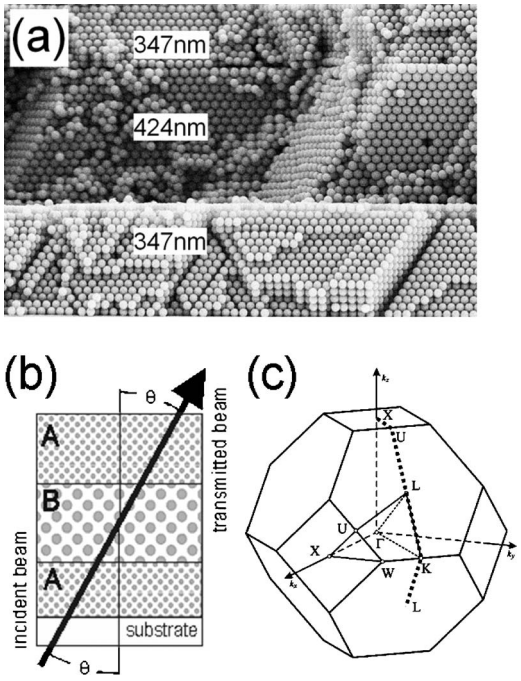

FIG. 1. (a) Scanning electron micrograph of the *ABA* hetero-opal, (b) schematic of transmission measurements in the *ABA* triple-film hetero-opal, and (c) the first Brillouin zone of the fcc lattice. The thick dashed line shows the scanning direction *XULKL'*.

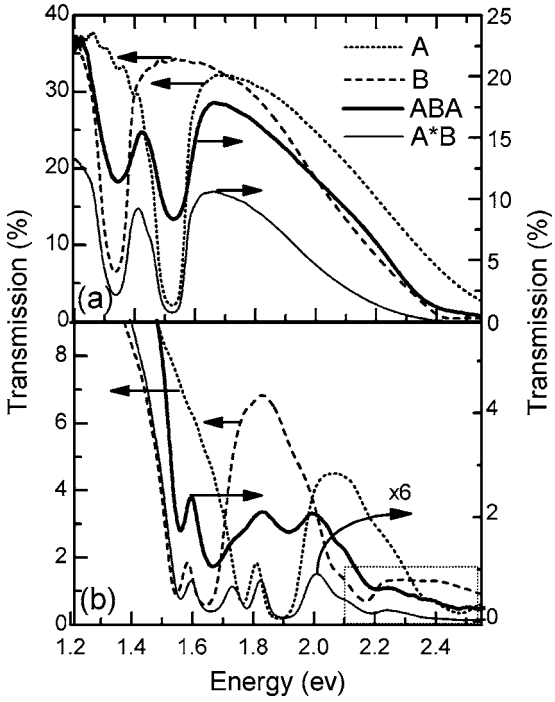

FIG. 2. Transmission spectra of the *ABA* triple-film opal in comparison with the spectra of its constituent *A* (dotted lines) and *B* (dashed lines) films at $\theta=0°$ (a) and 50° (b). At $\theta=50°$ the *A* $(11\bar{1})$ and *B* (111) bands overlap in the energy range from 1.65 to 1.75 eV.

opal films and the hetero-opal are given. In Sec. VI the possible mechanisms of transmission modification are discussed. Our results are then summarized in Sec. VII.

II. EXPERIMENTAL TECHNIQUE

The polymethyl methacrylate (PMMA) spheres were synthesized using the modified surfactant-free emulsion polymerization technique.[22,23] The opal films were prepared by vertically drawing a hydrophilic glass substrate from a suspension of PMMA beads, leading to the crystallization of opals in the moving meniscus.[13] The single- and triple-film opals were prepared from beads *A* and *B* with diameters of $D=374$ and 424 nm, respectively. A scanning electron micrograph of the cleaved *ABA* hetero-opal shows that opal films are properly crystallized and the interfaces do not give rise to defects, which propagate through the whole thickness of the films [Fig. 1(a)].

Angle-resolved transmission was used to measure the light propagation since it probes the whole thickness of a sample and accumulates all possible optical losses therein. The well-collimated beam of white light from the tungsten halogen lamp was focused onto the samples through a telescope. The diameter of the incident light beam was ~1 mm. The angle of incidence, θ, was measured from the film normal and the angle of detection was set equal to the angle of incidence [Fig. 1(b)]. The transmitted light was collected from a solid angle of 3° to allow acquisition of angle-resolved spectra. A charge coupled device spectrometer with a fixed grating was used. The spectra were collected using *s*-polarized light. A prism polarizer was placed in front of the sample to select the *s*-polarized light and a $\lambda/4$ plate behind the sample to convert the linear polarized light into circular polarization before entering the spectrometer. The samples were mounted on the rotating table with glass substrates facing the incident beam to allow transmission measurements at different angles θ in the range from −80° to +80°. The orientation of the samples was adjusted according to the surface diffraction pattern of an incident laser beam[24] so as to probe the PBG structure along the *XULKL'* line of the Brillouin zone of the fcc lattice [Fig. 1(c)].

III. TRANSMISSION SPECTRA

Figure 2 shows transmission spectra of *A* and *B* single-film opals, *ABA* triple film, and $A*B$ superposition at (a) $\theta=0°$ and (b) $\theta=50°$. The transmission minima appear due to light attenuation at the PBGs.

The weak Fabry–Pérot (FP) oscillations in the transmission, which are seen at the low frequency edges of the transmission spectrum of the films A and B [Fig. 2(a)], were used to determine the film thickness, t, using the expression $t=1239/2n_{\mathrm{eff}}\Delta E_{\mathrm{FP}}$, where ΔE_{FP} is the period of FP oscillations. The effective refractive index, $n_{\mathrm{eff}}=1.36$, was obtained from $n_{\mathrm{eff}}^2=n_{\mathrm{sphere}}^2 f_{\mathrm{sphere}}+n_{\mathrm{air}}^2(1-f_{\mathrm{sphere}})$, where f_{sphere} is the volume fraction of the structure occupied by PMMA spheres. Since $f_{\mathrm{sphere}}=0.74$ in the fcc lattice and $n_{\mathrm{sphere}}(\mathrm{PMMA})=1.489$, $t\approx 8.4$ μm applies for both single films. This value corresponds to 30 and 25 ML of beads, which form the (111) planes in the lattice of films *A* and *B*, respectively.

The transmission attenuation at the minimum, ΔI_0, in the spectrum obtained at $\theta=0°$ is related to the film thickness[25] through $t=-\ln(1-\Delta I/I_0)L_B$, where $\Delta I/I_0$ is the relative attenuation of the incident light with intensity I_0 at the central frequency of the Bragg gap, E_0, and L_B is the Bragg attenu-

ation length. The expression[25] $\Delta E/E_0=1.632D/\pi L_B$ links the band gap width and the attenuation length; ΔE is the PBG bandwidth. Assuming the relative gap bandwidth calculated for an infinitely large fcc crystal of the same refractive index contrast[26] as $\Delta E/E_0=0.056$, the attenuation length, L_B, is 3.2 μm for the film *A* and 3.9 μm for the film *B*. Correspondingly, $t=8.8$ μm for film *A* and $t=6.6$ μm for film *B* apply. The difference in film thickness obtained from FP oscillation calculation and from attenuation can be explained by assuming higher disorder in the lattice of the film *B* compared to that in the film *A*. It should be noted that the thickness obtained from FP oscillations is more accurate since n_{eff} is less dependent on disorder compared to L_B. The relative width of the Bragg gap is 7.40% for film *A* and 7.36% for film *B* [Fig. 2(a)]. This broadening, compared to the expected 5.6% relative bandwidth, is a consequence of the reduced thickness of opal films[26] and the lattice imperfections.[27]

At oblique light incidence, the transmission spectra of opal films become more complicated due to simultaneous contributions of different PBGs to the transmission attenuation [Fig. 2(b)]. The opposite dispersion of transmission minima related to the diffraction at different crystal planes allows PBGs to overlap along certain directions for the light traversing the hetero-opal. Moreover, these spectra are also more vulnerable to lattice disorder due to the increased optical path length.

At $\theta=0°$ the transmission spectra of the triple-film opal show two minima corresponding to attenuation of the incident light, successively, in both *A* and *B* films [Fig. 2(a)]. The transmission outside the PBG minima decreases with increasing frequency at approximately the same rate in triple- and single-film opals, which indicates similar lattice randomization. The relative minima bandwidth in the hetero-opal is 9.46% (10.83%) for the film *A* (*B*). From the relative attenuation, the total thickness of the two *A* films is deduced to be about 4.6 μm [18 (111) sphere ML] and the thickness of the *B* film −4.7 μm (15 ML). This yields the total *ABA* thickness of 9.3 μm. These numbers are in a reasonable agreement with the scanning electron microscopy (SEM) image shown in Fig. 1(a), which shows 16 and 9 sphere ML for the two outer A films and 17 ML for the B film. The difference between SEM and optical data is due to the variation in the film thicknesses across the sample. The transmission minima broadening observed in the triple-film opal as compared to that of single films is probably a consequence of smaller thickness of films *A* and *B* in the *ABA* hetero-opal.

Looking at the spectrum of the *ABA* hetero-opal obtained along the film normal, one can imagine that it resembles the superposition of transmission spectra of *A* and *B* films [Fig. 2(a)]. At the angle corresponding to the direction toward the edge of the Brillouin zone, the triple-film opal transmission spectrum possesses minima that are shifted and/or reduced in attenuation magnitude compared to the superposition spectrum. The effect is most pronounced in the frequency range from 1.60 to 1.80 eV [Fig. 2(b)], where the minima of *A* and *B* films overlap. We stress that the dips in transmission at 1.55 and 1.78 eV should have similar attenuation depth judging from the film thickness. Thus, the reduction in transmission suppression at the 1.78 eV minimum in the spectrum of the triple-film opal cannot be explained by poor resolution of the experimental setup and should therefore be assigned to the properties of the triple-film opal itself.

The principal difference between the spectra of single-film opals and the triple-film opal is the overall reduction in the transmission occurring at oblique light incidence due to the overlap of many transmission minima [see Fig. 2(b)]. This reduction may lead to the smoothing of the minima in transmission spectra, but it cannot produce new features. In contrast, additional minima were observed in the high frequency range, marked by the dotted rectangle.

IV. OVERVIEW OF TRANSMISSION CHANGES

It is instructive to consider the transmission surfaces, namely, the 3D plots of transmission as a function of incidence angle and wavelength, which give an impression of the transmission magnitude and minima dispersion simultaneously. The similarity of the overall superimposed transmission surface and that of the triple-film opal is obvious [Figs. 3(a) and 3(b)].

At frequencies below 1.60 eV the transmission surface of triple-film opal resembles that of superposition, as shown in Fig. 3. The most prominent features in this spectral range are the two consecutive branches of minima and the avoided crossing of the photonic bands at the edge of the Brillouin zone for film B. This observation points to the photonic band gap model as a better approximation of the observed transmission behavior compared to the diffraction model.

In the range of 1.60–1.80 eV, the deviation of the experimental data from the superposition spectra becomes visible at the angle range, where the PBGs of individual single films overlap. This deviation acquires the form of erasing the attenuation related to the film A from the transmission surface of the hetero-opal in comparison with the superposition transmission surface. Similar disappearance of transmission attenuation of film A occurs in the frequency range from 1.80 to 2.20 eV, as indicated by the symbol *xxx* in Fig. 3(a). Similar observations are made for the high frequency range from 2.25 to 2.55 eV as marked by the symbols *x* and *xx*, accordingly. It should be noted that the transmission of the triple-film opal changes within two orders of magnitude, whereas the superimposed transmission spans over five orders of magnitude.

Figure 4 shows the interface transmission function obtained by dividing the transmission surface of the triple-film opal by that of the superposition. Outside the diffraction resonances, the interface transmission increases by approximately three orders of magnitude with increasing angle of incidence. This effect can be explained by the reflectance of propagating light at the film interfaces. In terms of the effective RI, the *A* and *B* films are similar, and reflectance does not take place at the interfaces. Correspondingly, the *ABA* film contains two reflecting opal-air interfaces and the $A*B$ superposition takes into account four such interfaces. The interface transmission in the hetero-opal shows also the peaks at the transmission minima of the superposition spectra. As a result, the effective light attenuation is decreased for

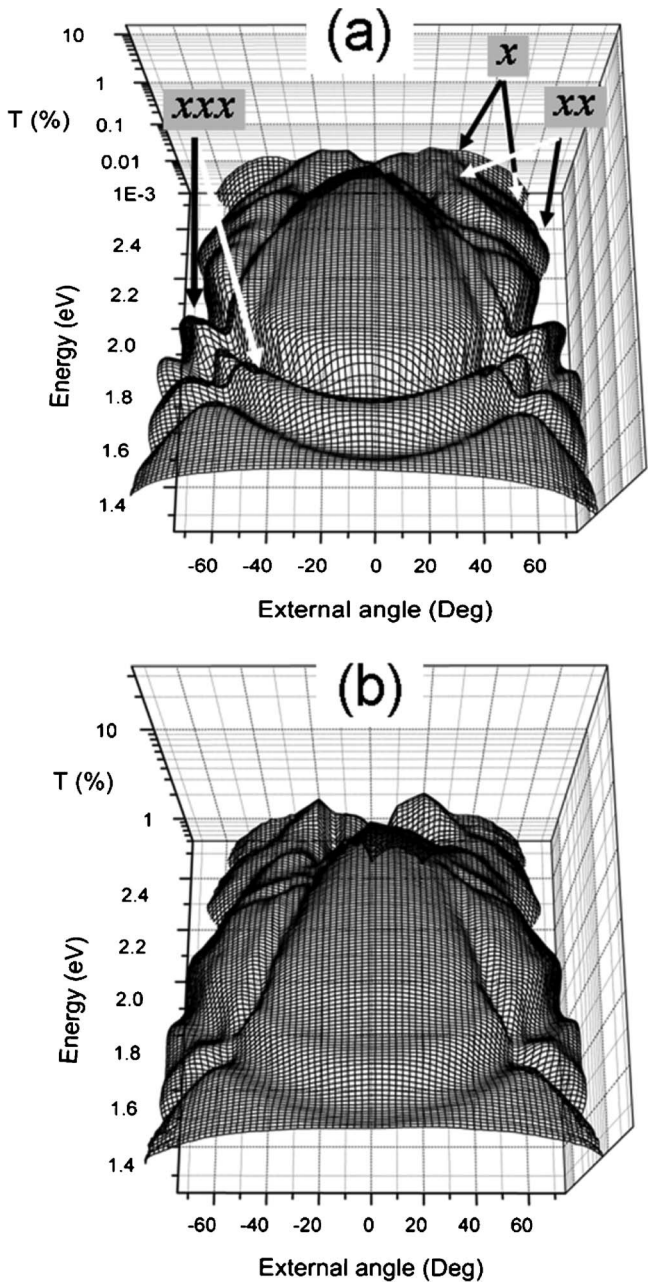

FIG. 3. Transmission surfaces obtained along LUX (0° to −74°) and LKL' (0°–74°) directions for the (a) $A*B$ superposition and (b) triple-film hetero-opal. The lines marked by x, xx, and xxx indicate branches of the transmission minima that appear in the transmission surface of the superposition but erased in the transmission surface of the triple-film opal.

the (111) minima of the triple-film opal as compared to similar minima in separate A and B films of the same thickness. Interestingly, the reduction applies most strongly to the attenuation of the (111) resonance of film A at high incidence angles. In contrast, the attenuation at high-order gaps in the triple-film opal is much less affected by heterostructuring [see inset to Fig. 4]. The latter effect needs more thorough theoretical investigation, but it is apparent that the reason for such transformation is similar to the application of a nonreflecting coating.

Figures 5(a) and 5(b) show the expanded view of a fraction of the transmission surfaces of Figs. 3(a) and 3(b), respectively, in the energy range of 2.25–2.55 eV and the angle

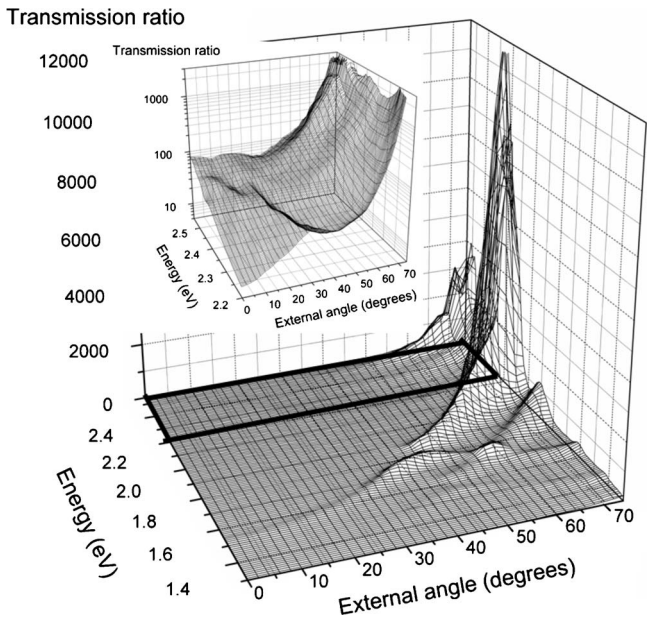

FIG. 4. Transmission surface of the interface transmission function. The inset shows an enlarged view of a fraction of the interface transmission function marked by the black rectangle.

range of 30°–74° in order to highlight the additional branches of minima that appear in the transmission surface of the triple-film opal. Dashed white lines in Fig. 5(a) indicate, in correspondence with Fig. 3, two minima branches marked as x and xx in the superposition transmission surface, where only one x branch is observed in the transmission surface of the triple-film opal. On the other hand, new minima appear in the range of (energy, angle of incidence)=(2.20–2.35 eV, 40°–60°) and (2.40–2.45 eV, 50°–65°) marked, respectively, by the numbers 1 and 2 in Fig. 5(b). This observation points to the fact that the formation of new transmission features occurs selectively with respect to the frequency and the wave vector of the propagating light.

V. DISPERSION OF TRANSMISSION MINIMA

Figure 6 plots the angular dispersion of central frequencies of transmission minima in the angle range of 0°–80°, which corresponds to scanning along the LKL' line on the surface of the first Brillouin zone of the fcc lattice, and 0° to −80°—the LUX line [see Fig. 1(c)]. In terms of the diffraction model, the low frequency transmission minima originate from the zero-order diffraction at the (111) and $(11\bar{1})$ or (002) family of planes, depending on the lattice orientation with respect to the plane of the light incidence. The dispersion of the diffraction resonance at (hkl) crystal planes is described by the Bragg law:

$$\lambda_{hkl} = 2d_{hkl}n_{\text{eff}}\sqrt{1-\sin^2 r_{hkl}}, \tag{1}$$

where d_{hkl} is the interplanar distance along the $[hkl]$ direction and r_{hkl} is the internal angle between the wave vector of the incident light and the $[hkl]$ vector. The external incidence angle θ is related to the internal angle r_{hkl} via the Snell law: $n_{\text{eff}}\sin(r_{hkl}) = n_{\text{air}}\sin(\theta)$.

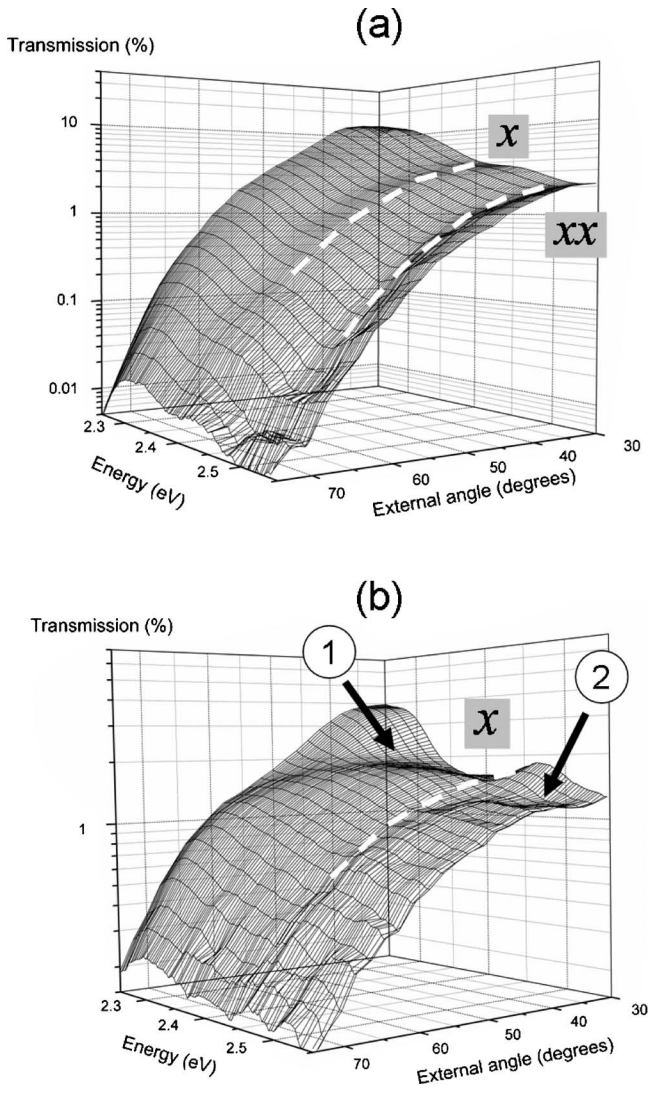

FIG. 5. Detailed view of transmission surfaces of Fig. 3 in the frequency and angle range of 2.25–2.55 eV and 30°–74°, respectively. The traces *x* and *xx* indicate the branches of the transmission minima, of which the branch *xx* is not observed in the hetero-opal. The numbers show the appearance of additional features in the transmission surface of the hetero-opal.

The experimental dispersion of the transmission minima in the single films *A* and *B* was fitted using expressions for resonances at the (111), (11$\bar{1}$), (002), and (200) planes with d_{hkl} and n_{eff} as the fitting parameters. These parameters are summarized in Table I. The difference between the sphere diameter obtained from the fit and the mean sphere diameter is $<2\%$. The lower n_{eff} obtained from the fit of the (111) diffraction minima, as compared to 1.36 from the effective medium approximation, can be explained by the porous nature of the spheres. Since the midfrequency of the (111) diffraction minimum does not change with the azimuth orientation of the incidence plane with respect to the opal lattice and is therefore independent of misalignment in crystallite lattices, the estimated values are reasonably accurate and can be used to calculate the dihedral angle,Λ_{hkl}, i.e., the angle between the (111) plane and the (11$\bar{1}$), (002), and (220) planes.

The dispersion of transmission minima in the triple-film opal is plotted on top of the dispersions of the constituent single films [Fig. 6]. The dashed lines represent the Bragg fit

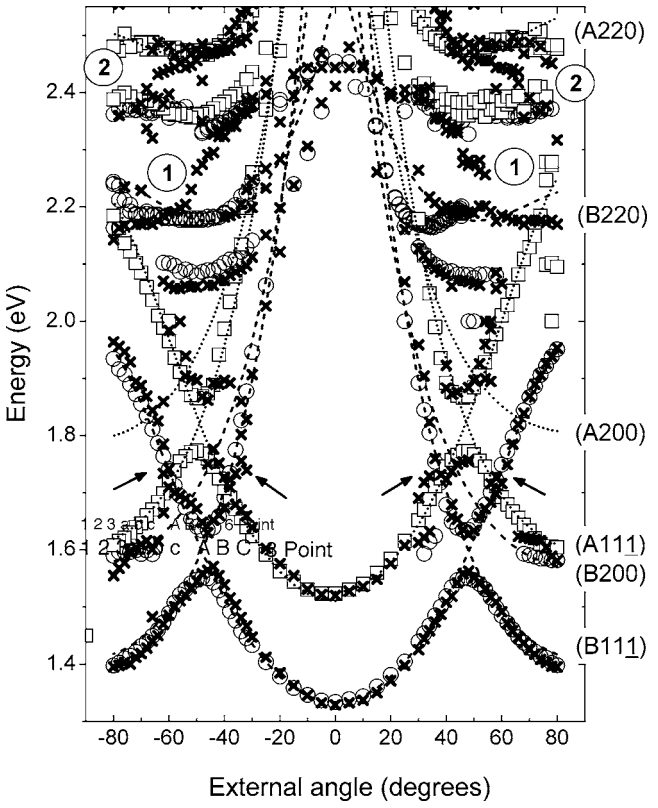

FIG. 6. Dispersion of transmission minima in the triple-film opal (crosses), in the opal film *A* (squares) and in the opal film *B* (circles). The Bragg fits are plotted for the (111), (11$\bar{1}$), (002), and (220) diffraction resonances (lines) as indicated. Numbers 1 and 2 denote the corresponding new features shown in Fig. 5(b).

with fitting parameters highlighted in bold in Table I. In the dispersion plot, the disappearance and emergence of minima in the transmission of the hetero-opal can be clearly seen. In the angle ranges $\pm(30-50°)$ and $\pm(60-80°)$, the transmission minima originating from the diffraction at the (111) and (11$\bar{1}$) and/or (002) for the film *A*, i.e., the band gap between fifth and sixth modes of the opal *A*-PhC, are almost completely erased. The disappearance of the transmission minima branches marked by *xx* in Fig. 5 in the triple-film opal transmission is evident. On the other hand, additional branches of minima appear in the angle range $\pm(30-70°)$ at energies greater than 2.10 eV, which do not belong to either of the single films. These branches are indicated by numbers 1 and 2 in correspondence with Fig. 5(b).

TABLE I. Parameters obtained from fitting experimental dispersion of transmission minima to the corresponding diffraction at the (111), (11$\bar{1}$), (002), and (200) planes according to the Bragg law, where *D* is the diameter of PMMA particle, n_{eff} is the, effective RI, and Λ is the angle that (11$\bar{1}$), (002), and (200) planes make with the (111) plane. The parameters highlighted in bold correspond to the Bragg fit plotted in Fig. 6.

	LKL′		*LUX*	
PD	D/n_{eff}	Λ	D/n_{eff}	Λ
[111]	421.8/1.35		421.8/1.35	
[11$\bar{1}$]	431.9/1.35	67.2	431.3/1.38	67.3
[002]	418.1/1.34	59.0	417.2/1.38	60.4
[220]	421.1/1.36	35.2	412.3/1.39	32.3

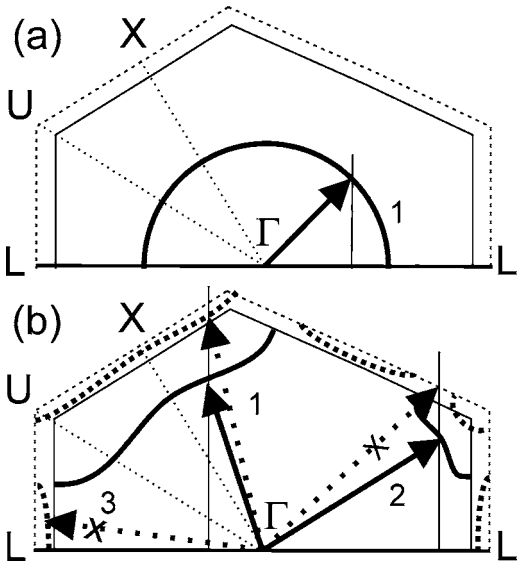

FIG. 7. The schematic of light refraction at the *B*-*A* interface in the hetero-opal. (a) Isofrequency contours of light at a frequency well below the lowest order PBG in *A* and *B* opals superimposed on the Brillouin zone sections of *B* (solid line) and *A* (dashed line) opals. The arrow stands for the *k* vector of the incident light. There is no refraction at the interface, because n_{eff} is the same for both films. (b) Isofrequency contours of *B* (thick solid lines) and *A* (thick dashed lines) opals at a frequency in the lowest order PBG range. The solid (dashed) arrows show *k* vectors of light propagating in the opal *B* (a). Case 1 represents the light refraction at the *B*-*A* interface. Cases 2 and 3 demonstrate blocking of the light propagation by the directional PBG in the *A* and *B* opals, respectively.

In addition, a slight shift of transmission minima, indicated by arrows, is observed in the triple-film opal at the spectral and angle range where the transmission minima of the two single films overlap. It is also worth noting that the attenuations of the transmission minima in the high frequency part of the dispersion diagram are rather weak but traceable.

VI. DISCUSSION

In the spectral range outside the PBG, there is no light reflection and refraction at the PhC interfaces of the hetero-crystal because the triple-film opal consists of components with the same effective RI. In addition, the interface roughness is unlikely to cause additional features in the transmission, since random scattering cannot provide the observed spectral and directional selectivity of the transmission modification. Consequently, the source of transmission spectra alteration in triple-film hetero-opals is the uneven transmission function of the interface itself. In what follows, we will discuss qualitatively two specific mechanisms that affect the propagation of light in a photonic heterocrystal.

The formalism of isofrequency surfaces and contours[28] is an appropriate tool to visualize light refraction at PBG interfaces. The isofrequency contour is the cross section of the PBG diagram at a fixed frequency [Fig. 7]. The A and B opal films possess the same n_{eff} at frequencies well below the lowest order PBG and thus there is no refraction at the interface because the normal components of the *k* vectors are equal at both sides of the interface [Fig. 7(a)].

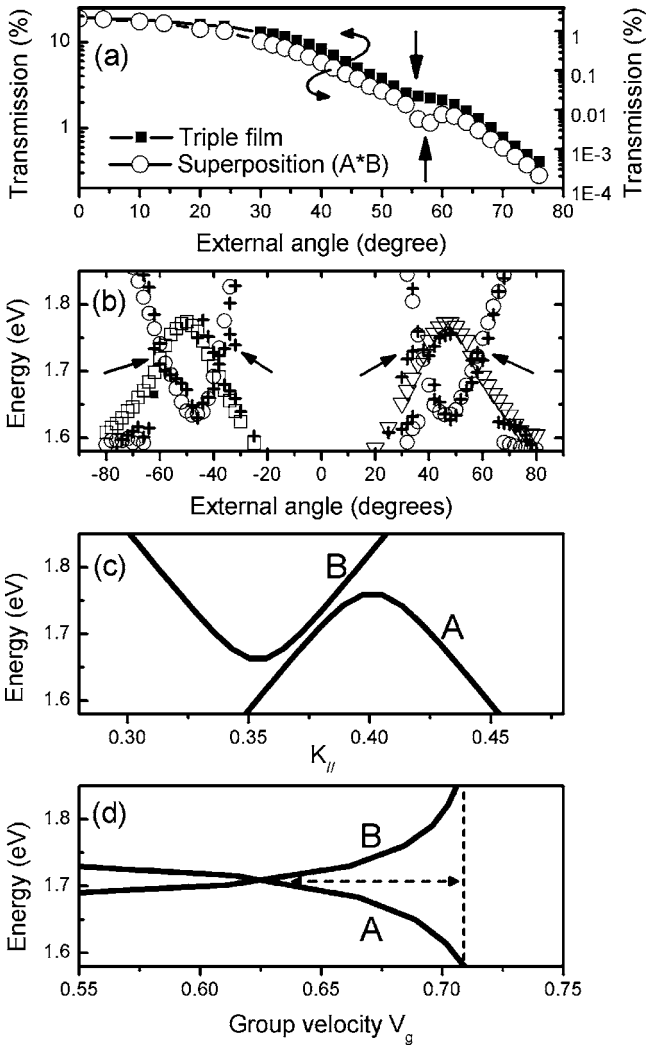

FIG. 8. (a) Transmission at the (111) diffraction minima of the film *B*: in the triple-film opal (filled squares) and in the superposition spectra (open circles); (b) a close-up plot of Fig. 6 for the spectral range of 1.60–1.85 eV; (c) and (d) show the calculated corresponding mode dispersions and group velocities for the *A* and *B* films, respectively.

In the frequency range of the PBG, the difference in the lattice parameters leads to the different topologies of isofrequency contours in *A* and *B* opals at the same frequency. In the case of semi-infinite PhCs, the light propagation through the interface is forbidden along the directions where the PBG of either film *A* or film *B* blocks the propagation [vectors 2 and 3 in Fig. 7(b)]. Hence, a larger fraction of the solid angle is forbidden for light propagation in the triple-film PhC compared to the single-film PhC. If the propagation is allowed, the refraction takes place due to different topologies of the isofrequency contours in the *A* and *B* opals [Fig. 7(b), vector 1]. This means that the light propagation direction in film *B* differs from that in the opal film *A* and this difference changes with the frequency and depends on the lattice constant ratio between films *A* and *B*. Hence, this refraction at the interface may explain the mismatch between the superposition of the transmission minima dispersion in the single *A* and *B* films and their dispersion in the hetero-opal.

Figure 8(a) plots the transmission at the (111) diffraction minima of film *B* in the triple-film opal, and associated su-

perposition spectra. The two curves possess similar shape, but with the minima shifted relative to each other, as indicated by the arrows. This shift occurs when the (111) dispersion branch of film *B* crosses the $(11\bar{1})$ branch of film *A*.

The observed shift can be explained by taking into account a decrease in the mode group velocity that takes place in the vicinity of the PBG. In PhCs with a directional PBG, this effect leads to a step in the group velocity profile at the interface. The sharp modulation takes place along the directions for which the PBGs in films *A* and *B* overlap. For example, this happens at frequencies between 1.60 and 1.85 eV in the angle range from 40° to 60° [Fig. 8(b)]. The calculated dispersion of PBG minima in this range is shown in Fig. 8(c) as a function of parallel wave vector. At these frequencies, the group velocity difference between the optical modes in films *A* and *B* becomes substantial and changes rapidly with the frequency. Moreover, in both crystals the group velocity is lower than the velocity in the medium with the effective index of refraction of the opal [Fig. 8(d)], due to an increase in the refractive index at the PBG edges.[29] The PhC of the heterostructure with the lower group velocity therefore limits the flux through the heterostructure at this frequency due to the conservation of the flux continuity. Correspondingly, the superseding part of the incident flow is partially back reflected at the interface, and becomes partially frozen in the standing wave.[30] Thus, the difference in the mode group velocities may obscure the PBG-induced locations of the transmission minima. This effect becomes especially strong in the case of a flat dispersion of eigenmodes[30] in films *A* and *B* and can explain the distortion of the observed dispersion of transmission minima corresponding to light with wave vectors directed toward the edges of the Brillouin zone [Fig. 8(b)].

The above arguments should be considered together with the issue of mode coupling at the interface, which proceeds through the interface light scattering.[25] The drawback of the approach discussed above is in neglecting the PhC thickness, which is needed for the development of the Bloch modes, and the spatial region required to couple the electromagnetic waves of the incident beam to the PhC eigenmodes. In the studied triple-film opal, this transition region can be compared to the opal film thickness. Therefore, strictly speaking, the wave propagation in film *B* cannot be considered independently from that in film *A* and vice versa. In the multiple-period hetero-PhC the superlattice approach was used to calculate the resulting PBG structure.[30] In the double- and triple-film opals this issue remains a matter of theoretical consideration.

Since coupling takes place between two restricted mode reservoirs, the overall transparency of the hetero-PhC may be reduced. This is because mode mismatch gives rise to the interface light scattering. Therefore, the overall smoothing of the transmission surface of the hetero-opal [see Fig. 3(b)] as compared to the superimposed transmission of the single-film opals could be a consequence of the interface mode mismatch. Additionally, scattered light excites interface modes, which transfer energy along the interface and thus reduce the transmitted light intensity. The latter losses are related to surface modes,[31] which exist at energies >3 eV, i.e., outside the studied range.

VII. SUMMARY

The transmission spectra of the *ABA* triple-film hetero-opal, which was assembled from single *A* and *B* opal films with slightly different lattice parameters, were measured with *s*-polarized light and compared to the spectra of its constituent films along the $XULKL'$ line on the surface of the fcc Brillouin zone. Comparison of the transmission attenuation and the dispersion of transmission minima demonstrated that the transmission spectra of the *ABA* triple-film opal can be, to a first approximation, described as a linear superposition of transmission properties of its constituent films. More detailed analysis shows (i) the disappearance of transmission minima originating from film *A* in the energy range from 1.85 to 2.20 eV, and (ii) the formation of the additional branches of minima in the range from 2.20 to 2.55 eV.

The interface transmission function was extracted from the comparison between the experimental transmission spectra of the *ABA* hetero-opal PhC and the single *A* and *B* films. It is instructive to note here that the overall dissimilarity between the *ABA* hetero-opal transmission and the $A*B$ superposition transmission appears due to the difference in the boundary conditions at the PhC film interfaces in the hetero-opal and in the single films. It is worth noting that the effect is stronger for the PBG spectral intervals, where the actual RI exceeds the effective RI of the opal. Hence, the interface transmission function emphasizes the spectral regions with specific coupling conditions for the light traversing the interface between different PBG materials.

The observed dissimilarities, which appear only at specific spectral intervals and along specific propagation directions, suggest the selectivity of the interface transmission in the hetero-opal. The frequency-dependent light coupling conditions at the internal interfaces and the mismatch in mode group velocities in the hetero-opal components were considered as the reasons for the uneven interface transmission spectrum.

These observations demonstrated the possibility for purposeful engineering of light propagation in finite-size complex multilayered heterogeneous PBG materials.

ACKNOWLEDGMENTS

This paper was based upon work supported by the Science Foundation Ireland under Grant No. 02/IN.1/172. The authors also wish to acknowledge support from the EU IST project "PHAT," the EU Network of Excellence (NoE) "PHOREMOST," and the Russian RFBR project 05-02-16975-?

[1] S.-Y. Lin, J. G. Fleming, D. L. Hetherington, B. K. Smith, R. Biswas, K. M. Ho, M. M. Sigalas, W. Zubrzycki, S. R. Kurtz, and J. Blur, Nature (London) **394**, 251 (1998); J. G. Fleming and S.-Y. Lin, Opt. Lett. **24**, 49 (1999).
[2] S. Noda, K. Tomoda, N. Yamamoto, and A. Chutinan, Science **289**, 604 (2000).
[3] S. Kawakami, O. Hanaizumi, T. Sato, Y. Ohtera, T. Kawashima, N. Yasuda, Y. Takei, and K. Miura, Electron. Commun. Jpn., Part 2: Electron.

82, 43 (1999).
[4]M. Campbell, D. N. Sharp, M. T. Harrison, R. G. Denning, and A. J. Turberfield, Nature (London) **404**, 53 (2000); Y. V. Miklyaev, D. C. Meisel, A. Blanco, G. von Freymann, K. Busch, W. Koch, C. Enkrich, M. Deubel, and M. Wegener, Appl. Phys. Lett. **82**, 1284 (2003).
[5]K. Aoki, H. T. Miyazaki, H. Hirayama, K. Inoshita, T. Baba, K. Sakoda, N. Shinya, and Y. Aoyagi, Nature (London) **2**, 117 (2003).
[6]M. Deubel, G. von Freymann, M. Wegener, S. Pereira, K. Busch, and C. M. Soukoulis, Nature (London) **3**, 444 (2004).
[7]P. N. Pusey and W. van Megen, Nature (London) **320**, 340 (1986); P. N. Pusey, W. van Megen, P. Bartlett, B. J. Ackerson, J. G. Rarity, and S. M. Underwood, Phys. Rev. Lett. **63**, 2753 (1989).
[8]A. P. Gast and Y. Monovoukas, Nature (London) **351**, 553 (1991).
[9]Y. Xia, B. Gates, Y. Yin, and Y. Lu, Adv. Mater. (Weinheim, Ger.) **12**, 693 (2000).
[10]K. Busch and S. John, Phys. Rev. E **58**, 3896 (1998); A. Blanco, E. Chomski, S. Grabtchak, M. Ibisate, S. John, S. W. Leonard, C. Lopez, F. Meseguer, H. Miguez, J. P. Mondia, G. A. Ozin, O. Toader, and H. M. van Driel, Nature (London) **405**, 437 (2000); Yu. A. Vlasov, X.-Z. Bo, J. C. Sturm, and D. J. Norris, *ibid.* **414**, 289 (2001).
[11]S. G. Romanov, H. M. Yates, M. E. Pemble, and R. M. De La Rue, J. Phys.: Condens. Matter **12**, 8221 (2000).
[12]P. Jiang, G. N. Ostojic, R. Narat, D. M. Mittleman, and V. L. Colvin, Adv. Mater. (Weinheim, Ger.) **13**, 389 (2001).
[13]R. Rengarajan, P. Jiang, D. C. Larrabee, V. L. Colvin, and D. M. Mittleman, Phys. Rev. B **64**, 205103 (2001).
[14]M. Egen, R. Voss, B. Griesebock, R. Zentel, S. G. Romanov, and C. M. Sotomayor Torres, Chem. Mater. **15**, 3786 (2003).
[15]N. Gaponik, A. Eychmüller, A. L. Rogach, V. G. Solovyev, C. M. Sotomayor Torres, and S. G. Romanov, J. Appl. Phys. **95**, 1029 (2004).
[16]Y. Zhao, K. Wostyn, G. de Schaetzen, K. Clays, L. Hellemans, A. Persoons, M. Szekeres, and R. A. Schoonheydt, Appl. Phys. Lett. **82**, 3764 (2003).
[17]N. Tetreault, A. Mihi, H. Miguez, I. Rodriguez, G. A. Ozin, F. Meseguer, and V. Kitaev, Adv. Mater. (Weinheim, Ger.) **16**, 346 (2004).
[18]S. G. Romanov, N. Gaponik, A. Eychmüller, A. L. Rogach, V. G. Solovyev, D. N. Chigrin, and C. M. Sotomayor Torres, *Photonics Crystals*, edited by K. Busch, S. Lolkes, R. Wehrspohn, and H. Foll (Wiley, Weinheim, 2004), pp. 132–152.
[19]E. Pavarini, L. C. Andreani, C. Soci, M. Galli, F. Marabelli, and D. Comoretto, Phys. Rev. B **72**, 045102 (2005).
[20]E. Istrate, M. Charbonneau-Lefort, and E. H. Sargent, Phys. Rev. B **66**, 075121 (2002).
[21]S. G. Romanov, D. N. Chigrin, C. M. Sotomayor Torres, N. Gaponik, A. Eychmüller, A. L. Rogach, M. Egen, and R. Zentel, Proc. SPIE **5450**, 44 (2004).
[22]M. Müller, R. Zentel, T. Maka, S. G. Romanov, and C. M. Sotomayor Torres, Chem. Mater. **12**, 2508 (2000).
[23]M. Egen and R. Zentel, Chem. Mater. **14**, 2176 (2002).
[24]F. Garcia-Santamaria, J. F. Galisteo-Lopez, P. V. Braun, and C. Lopez, Phys. Rev. B **71**, 195112 (2005).
[25]S. G. Romanov, C. M. Sotomayor Torres, M. Egen, and R. Zentel, Photonics Nanostruct. Fundam. Appl. **4**, 59 (2006).
[26]J. F. Bertone, P. Jiang, K. S. Hwang, D. M. Mittleman, and V. L. Colvin, Phys. Rev. Lett. **83**, 300 (1999).
[27]J. F. Galisteo Lopez and W. L. Vos, Phys. Rev. E **66**, 036616 (2002).
[28]M. Notomi, Phys. Rev. B **62**, 10696 (2000).
[29]J. F. Galisteo-Lopez, M. Galli, M. Patrini, A. Balestreri, L. C. Andreani, and C. Lopez, Phys. Rev. B **73**, 125103 (2006).
[30]E. Istrate and E. H. Sargent, Rev. Mod. Phys. **78**, 455 (2006).
[31]S. G. Romanov, M. Bardosova, M. Pemble, and C. M. Sotomayor Torres, Appl. Phys. Lett. **89**, 043105 (2006).